Limitations of the Förster Description of Singlet Exciton Migration: The Illustrative Example of Energy Transfer to Ketonic Defects in Ladder-type Poly(*para*-phenylenes)**

By *Herbert Wiesenhofer*,* *David Beljonne*, *Gregory D. Scholes*, *Emmanuelle Hennebicq*, *Jean-Luc Brédas*, and *Egbert Zojer**

Energy-transfer processes in phenylene-based materials are studied via two different approaches: i) the original Förster model, which relies on a simple point-dipole approximation; and ii) an improved Förster model accounting for an atomistic description of the interacting chromophores. Here, to illustrate the impact of excited-state localization and the failure of the point-dipole approximation, we consider a simple model system which consists of two interacting chains, the first a pristine ladder-type poly(*para*-phenylene) (LPPP) chain and the second an LPPP-chain bearing a ketonic defect. The latter chain displays both localized electronic excitations close to the ketonic sites as well as excited states that are delocalized over the whole conjugated chain. Singlet hopping rates have been computed for energy transfer pathways involving these two types of excitations. A generalized Förster critical distance is introduced to account for the errors associated with averaging out the actual molecular structures in the original Förster model.

1. Introduction

Energy transfer is involved in the conversion of solar energy by many biological systems such as bacteria, algae, and plants.[1,2] It is a key process in the working mechanism of many organic optoelectronic devices. For instance, it has been shown that by exploiting energy-transfer processes, it is possible to tune the emission color of polymer blends to realize multicolor light-emitting devices (LEDs).[3–6] On the other hand, undesired effects, such as the quenching of excitons or emission by chemical impurities,[7] are promoted by energy migration to such defects. It is therefore of importance to optimize energy migration in such a way as to efficiently drive excitations to luminescent centers in LEDs (or alternatively to dissociation centers in solar cells).

Experimental and theoretical studies have provided a rather detailed picture of the impact of chemical and structural defects on the excited-state dynamics of conjugated materials. In this context, Förster theory has played a central role. However, this theory was originally developed to account for resonance energy-transfer phenomena in dilute solutions. As a result, significant deviations are to be expected when the distance between the excited donor molecule (D*) and the acceptor (A) becomes similar to the size of the chromophore.[8–11] It is only when going beyond the limitation of the point-dipole approximation that, for example, the relative efficiencies of interchain versus intrachain energy transfer can be quantitatively modeled.[12]

To go beyond simple Förster theory usually requires the application of sophisticated quantum-chemical calculations. Here, we report the results of such calculations for model conjugated systems; we show that the actual energy-transfer rates,

[*] Prof. E. Zojer, H. Wiesenhofer
Institute of Solid State Physics
Graz University of Technology
Petersgasse 16, A-8010 Graz (Austria)
E-mail: egbert.zojer@chemistry.gatech.edu;
herbert.wiesenhofer@tugraz.at
Dr. D. Beljonne, E. Hennebicq
Chemistry of Novel Materials
University of Mons-Hainaut
Place du Parc 20, B-7000 Mons (Belgium)
Prof. G. D. Scholes
Department of Chemistry
University of Toronto
80 St. George Street, Toronto, Ontario M5S 3H6 (Canada)
Prof. E. Zojer, Dr. D. Beljonne, Prof. J.-L. Brédas
School of Chemistry and Biochemistry
Georgia Institute of Technology
Atlanta, GA 30332 (USA)

[**] The authors thank B. P. Krueger for stimulating discussions. The work in Graz benefits from the financial support by the Spezialforschungsbereich Elektroaktive Stoffe (Project F917) of the Austrian Fonds zur Förderung der Wissenschaftlichen Forschung. The work in Mons is partly supported by the Belgian Federal Government "Inter-University Attraction Pole in Supramolecular Chemistry and Catalysis (PAI 4/11)" and the Belgian National Fund for Scientific Research (FNRS-FRFC). The work at Georgia Tech is partly supported by the US National Science Foundation (through the STC for Materials and Devices for Information Technology Research and through CHE-0342321, the Office of Naval Research) and the Georgia Tech Center for Organic Photonics and Electronics. EH and DB are a research fellow and a senior research associate of the Belgian National Fund for Scientific Research (FNRS). GDS gratefully acknowledges the Natural Sciences and Engineering Research Council of Canada and Photonics Research Ontario for financial support.

 DOI: 10.1002/adfm.200400108

calculated using a more rigorous model based on donor and acceptor transition densities, critically depend on the specific electronic nature and spatial extent of the relevant excited states. Interestingly, it is found that for certain relative orientations between the donor and acceptor molecules, traditional Förster theory leads to a strong underestimation of the energy-transfer rates, while for other orientations it strongly overestimates the rates.

2. Description of the Energy-Transfer Process and Definition of a Generalized Förster Radius

A widely used expression for the energy-transfer rate (k) in Förster theory is written in terms of the Förster radius R_0, which defines the distance at which the energy-transfer efficiency is 50 %:[13]

$$k_{\text{Förster}} = \frac{1}{\tau_{\text{D}}}\left(\frac{R_0}{R}\right)^6 \tag{1}$$

with

$$R_0^6 = \frac{9000(l\ln 10)\kappa^2 \Phi_{\text{D}} I}{128\pi^5 N n^4} \tag{2}$$

where κ is the orientation factor associated with the point-dipole interaction between donor and acceptor (vide infra), R corresponds to their center-to-center separation in units of centimeters, and n is the refractive index of the intervening medium. N is Avogadro's number, Φ_{D} is the fluorescence quantum yield, and τ_{D} is the lifetime of the donor (in the same units as $1/k$). The Förster spectral overlap (I) is obtained from the overlap—on a wavenumber (or wavelength λ) scale—of an experimentally measured absorption spectrum for the acceptor (where intensity is in molar absorbance), with an area-normalized emission spectrum of the donor; I has units of $\text{M}^{-1}\,\text{cm}^3$:

$$I = \int_0^\infty \frac{a_{\text{A}}(\nu) f_{\text{D}}(\nu)}{\nu^4}\,\text{d}\nu \tag{3a}$$

$$I = \int_0^\infty a_{\text{A}}(\lambda) f_{\text{D}}(\lambda)\,\lambda^4\,\text{d}\lambda \tag{3b}$$

The practical advantage of the approach outlined above is that all involved quantities can be determined experimentally. The concept of a critical transfer distance has proven extremely useful as a universal characterization of resonant energy-transfer efficiency. However, this formulation of a critical transfer distance applies only to a point-dipole model for the electronic coupling between a donor–acceptor pair. That is, the Coulombic electronic coupling that mediates energy transfer is limited to the dipole–dipole term in a multipolar expansion of the interaction potential:[13]

$$V^{\text{Coul}} \approx V^{\text{dd}} = \frac{1}{4\pi\varepsilon_0}\frac{\kappa \mu_{\text{D}} \mu_{\text{A}}}{R^3} \tag{4}$$

Here κ, the orientation factor between the two point transition dipoles μ_{D} and μ_{A}, is given by:

$$\kappa = \vec{\mu}_{\text{D}}\vec{\mu}_{\text{A}} - 3\left(\vec{\mu}_{\text{D}}\vec{R}\right)\left(\vec{\mu}_{\text{A}}\vec{R}\right) \tag{5}$$

Such an approximation works when the intermolecular separation is large compared to molecular size, and leads to the familiar R^{-6} distance-dependence characteristic of the Förster equation. It is apparent from Equation 4 that the only molecular observables retained in Förster theory to characterize the involved excited states are the transition dipoles. Thus, importantly, such an approach does not account for the actual shape of the excited-state wavefunctions, such as their localized/delocalized character.

To consider properly the quantum-mechanical aspects of the energy-transfer process, one has to go beyond the above approximations. The nature of the excited states strongly influences the electronic coupling between the donor and the acceptor, which will be the focus of our discussion. We note that in general the electronic coupling consists of two parts: a long-range Coulomb interaction and short-range exchange and charge-transfer contributions. The latter requires wavefunction overlap between donor and acceptor and are therefore only relevant at very close intermolecular distances or when the Coulomb contributions are small such as in the case of symmetry or spin-forbidden transitions.

Within a zero-differential overlap (ZDO) formalism, the Coulombic part of the electronic coupling can, to first approximation, be estimated from atomic transition densities (in the form of multicentric monopole expansions),[10,14,15] which incorporate the specific spatial shapes of the various excited states:

$$V^{\text{Coul}} = \frac{1}{4\pi\varepsilon_0}\sum_{i,j}\frac{q_i q_j}{r_{ij}} \tag{6}$$

Here, q_i corresponds to the transition density associated with atom i at position r_i on the donor molecule and q_j is the transition density for atom j at position r_j on the acceptor molecule.

It is possible to define a generalized Förster critical distance R_{G} for a simple donor–acceptor pair. When inhomogeneity in the donor–acceptor transition frequencies is negligible, R_{G} can be related to the Förster critical distance according to:

$$R_{\text{G}} = \eta R_0 \tag{7}$$

The electronic coupling correction factor η is, as we show below, a function of the relative positions and orientations of the donor and acceptor molecules and of the actual shapes of the transition densities associated with the electronic excitations of interest. As the transfer rate is proportional to the square of the electronic coupling, V, one obtains from Equations 1, 2, and 7:

$$\eta = \left(\frac{V}{V^{\text{dd}}}\right)^{\frac{1}{3}} \tag{8}$$

with V being the actual electronic coupling between the donor and the acceptor (in our case Eq. 6) and V_{dd} the coupling obtained by the point-dipole model (Eq. 4).

ADVANCED FUNCTIONAL MATERIALS

3. Results and Discussion

We have chosen to study energy transfer in bridged poly(*para*-phenylene)-type materials in order to evaluate the impact of the presence of ketonic defects (Fig. 1). The latter are of practical importance, as energy transfer to ketonic defects is largely responsible for a shift of the emission to the green and

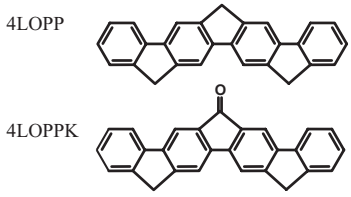

Figure 1. Chemical structure of selected model chromophores of ladder-type oligoparaphenylenes with (bottom) and without (top) ketonic defects at the central bridge.

for reduced efficiency in poly(*para*-phenylene)-based displays.[7,16–21] Moreover, the specific nature of the lowest excited states in ketone-containing poly(fluorenes) and ladder-type poly(*para*-phenylenes) makes them ideal candidates to study the details of energy migration in conjugated polymers: as the lowest two excited states in ketone-containing chains display an n–π* character and a charge-transfer CT–π–π* character, respectively; they are both localized in the vicinity of the ketonic defect. The third excited state is a delocalized π–π* state that is reminiscent of the lowest excited state in pristine, ketone-free chains.[16,21] If long-range Coulomb interactions prevail (see below), the optically weak n–π* state should hardly contribute to the singlet energy transfer, while both CT–π–π* and π–π* states are expected to provide efficient channels for energy transfer to ketone-bearing chains.

To investigate the effect of various geometric parameters, we considered two representative configurations, namely a head-to-head and a cofacial (sandwich) configuration (see right part of Fig. 4, later) between a donor chain and an acceptor chain. The donor is a four-ring ladder-type oligo(*para*-phenylene) (LOPP); it is characterized by a strongly allowed π–π* emission with an INDO/SCI-calculated vertical transition energy of 3.61 eV. As acceptors, various ladder-type oligo(*para*-phenylene) chains carrying a ketonic defect in the center (LOPPK) with chain lengths ranging from 4 to 14 rings have been considered; the INDO-SCI vertical absorption energies are given in Table 1.

Figure 2 shows the atomic transition density distribution for excitation into the CT–π–π* and π–π* states of a 14-ring acceptor. The crucial difference between the two states is that, while the former is localized largely on the central two rings, the latter is delocalized over the whole chain. In Figure 3, we display the dependence on intermolecular distance of the electronic coupling between a pristine four-ring LOPP (acting as the donor) and a 14-ring LOPPK bearing a ketonic defect (acting as the acceptor). Here, the two

Table 1. Calculated vertical singlet transition energies and oscillator strengths for absorption in different LOPPK acceptors as a function of the number of phenylene units.

	n–π*		CT–π–π*		π–π*	
Number of rings	*E* [eV]	Osc. strength	*E* [eV]	Osc. strength	*E* [eV]	Osc. strength
4	2.82	0.00	2.93	0.16	3.72	0.53
6	2.83	0.00	2.86	0.35	3.55	1.74
8	2.83	0.00	2.84	0.54	3.43	2.85
10	2.83	0.00	2.83	0.70	3.35	3.79
12	2.83	0.00	2.83	0.84	3.29	4.68
14	2.83	0.00	2.82	0.95	3.25	5.55

chromophores are arranged in a head-to-head geometric configuration, leading to a shortest considered distance of 40.3 Å between the molecular centers when assuming touching van der Waals' spheres for the terminal H-atoms of the two chains. As expected, the point-dipole method (Eq. 4) and the atomic transition density method (Eq. 6) yield similar results for very large inter-molecular distances. However, at shorter separations, the point-dipole approximation strongly underestimates the actual coupling with respect to the multicentric monopole expansion.

To highlight the differences between the transfer to the CT–π–π* state and the π–π* state, η, as defined by Equation 8, is displayed in the inset of Figure 3 (note that an η value of 1.55 for transfer to the delocalized state and 1.28 for transfer to the localized state at the shortest inter-molecular distances, correspond to ratios of the energy-transfer rates of 14.1 and 4.5, respectively.) The different behavior observed for the two migration channels reflects the different shapes of the associated transition densities: while the localized character of the CT–π–π* excited state (confined in the central part of the acceptor molecule) seems to justify the use of the point-dipole approximation at intermediate molecular separations, this approximation completely breaks down in the case of transfer to the delocalized π–π* state.

The influence of the shape of the molecular wavefunction is further illustrated by comparing the dependence of the electronic coupling on the acceptor size. This is shown in Figure 4. The upper part of Figure 4 corresponds to the donor and acceptor in a head-to-head configuration for the shortest intermolecular distance (touching van der Waals' radii of the terminal hydrogens). The increase in η with increasing acceptor length is much less pronounced for the localized CT–π–π*

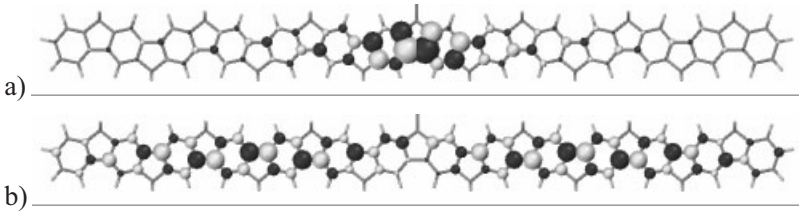

Figure 2. INDO/SCI calculated atomic transition densities for excitations to the localized CT–π–π* state (a) and to the delocalized π–π* state (b) in 14 LOPPK. The areas of the circles are chosen to be proportional to the atomic transition densities.

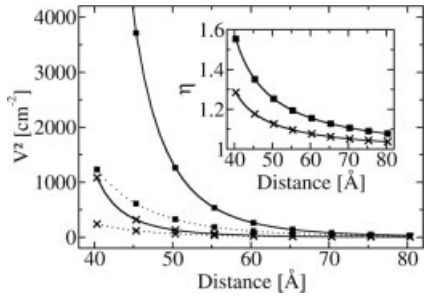

Figure 3. Distance dependence of the electronic coupling V^2 for energy transfer from a 4-ring LOPP donor to a 14-ring LOPPK acceptor (the energy-transfer rate k is directly proportional to V^2). The solid lines in the plots represent the results obtained from atomic transition densities (Eq. 6); the dotted lines are calculated using the point-dipole approximation (Eqs. 4,5). Solid squares describe energy transfer to the delocalized π–π* backbone states and crosses represent transfer to the localized CT–π–π* states. The insets shows the correction factor η (Eq. 8) for transfer into localized CT–π–π* (crosses) and delocalized π–π* (squares) states.

excited state compared to the delocalized π–π* state. This is again fully consistent with the fact that, in the context of energy-transfer processes, a localized transition density can be more reasonably described by a point dipole than a delocalized one. The lower part of Figure 4 demonstrates the complete failure of the point-dipole approximation for a cofacial arrangement.[11] Interestingly, while in the case of the head-to-head configuration, the point-dipole approximation is found to underestimate the electronic coupling, it leads to largely overestimated values in the case of cofacial arrangements.

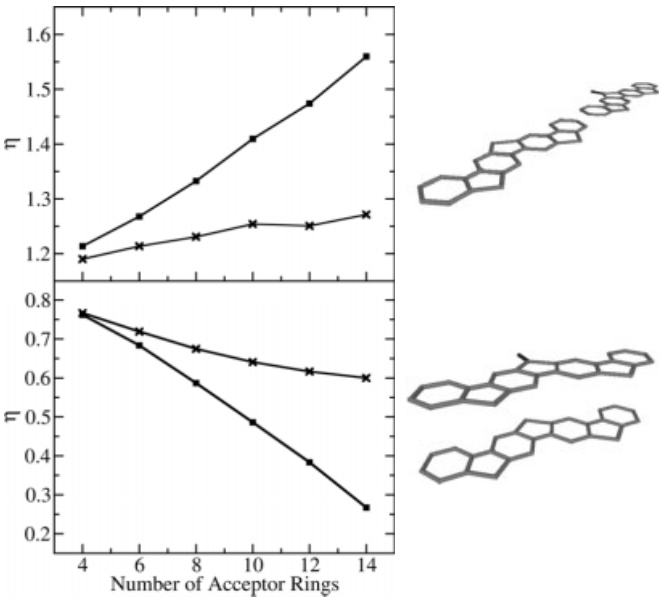

Figure 4. Correction factor η as a function of the size of the acceptor molecule for head-to-head configuration (top) and cofacial configuration (bottom). Solid squares: energy transfer to the delocalized π–π* acceptor state; Crosses: transfer to the CT–π–π* states localized close to the ketonic defects. In the head-to-head configuration, the inter-molecular distance is chosen in a way that the van der Waals' radii of the terminal hydrogens of the donor and acceptor chains touch. The inter-molecular distance for the cofacial conformation is chosen to be 10 Å to ensure that one is dealing with fully incoherent transfer, i.e., weak coupling limit (note that the oscillations in the plots arise from the two different positions of the terminal rings for different acceptor sizes, since they are not exactly aligned with the molecular axis in LOPPK).

This behavior can be qualitatively understood if one assumes, for the sake of simplicity, that the overall transition dipole of the donor (or the acceptor) can be partitioned into two dipoles arranged along the molecular axis, one located at 1/4 of the length and the second located at 3/4 of the length of the molecule[2,22] (see Fig. 5). The overall transition rate can now be expressed as a sum over all the contributions from the

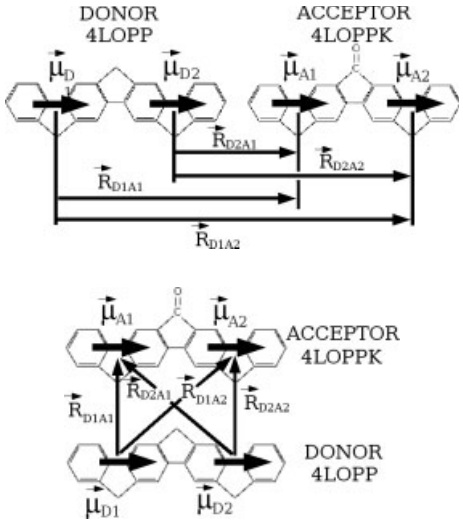

Figure 5. Schematic representation of the dipole interactions when considering split transition dipoles. Top: head-to-head configuration; bottom: cofacial configuration.

individual transition dipoles. From the $1/R^3$ dependence of the electronic coupling (Eq. 4), it is clear that for the head-to-head case the gain in coupling due to the closer lying transition dipoles is stronger than the loss due to the more distant ones. This explains the larger values for the coupling obtained with the distributed monopole method compared to the simple dipole approximation, which assumes that the dipoles are located at the centers of the molecules. For the cofacial configuration, one obtains the opposite trend since some of the interactions of the individual point dipoles can cancel one another. This is a result of the different orientational factors (Eq. 5) between certain pairs of interacting point dipoles in the lower part of Figure 5.[23] Moreover, the distance between certain pairs of dipoles is increased compared to the simple dipole model.

In an amorphous film, the head-to-head and cofacial conformations are only two limiting cases of the possible geometric arrangements. As an example, we have also evaluated V^2 a function of the angle between the donor and acceptor molecular axes (in this case, for a 4LOPP donor and a 4LOPPK acceptor) (see Fig. 6). The inset shows the corresponding η values. It is seen that in the range between 0° and about 100°, the dipole approximation (dotted lines) underestimates the electronic coupling, while it overestimates it for angles larger than about 100° ($\eta > 1$ for small angles and < 1 for large angles). These

ADVANCED FUNCTIONAL MATERIALS

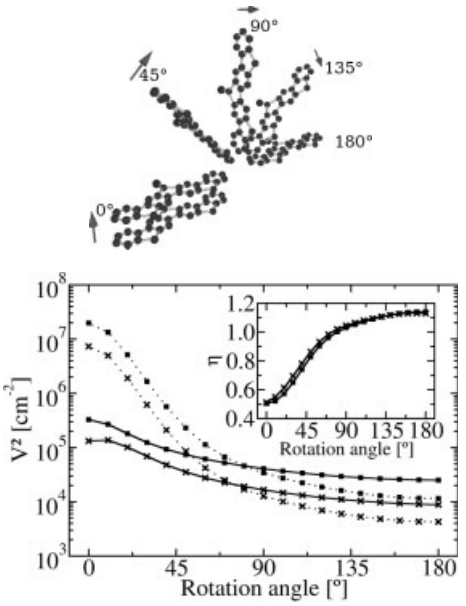

Figure 6. Electronic coupling V^2 as a function of the relative orientations of the donor and acceptor oligomers. The model system consists of a 4-ring LOPP donor and a 4-ring LOPPK acceptor with a distance between the molecular centers of 17.9 Å for the head-to-head configuration and 4.2 Å for the cofacial configuration. The acceptor is rotated from a cofacial configuration to a close to head-to-head configuration as shown in the upper part of the figure. The values for the angle between the donor and acceptor oligomers goes from 0° (cofacial configuration) to 180° (head-to-head configuration). Lines with solid squares denote transfer to the delocalized backbone states whereas lines with crosses refer to transfer to the localized CT–π–π* state. The relatively small size of the acceptor leads to minor differences for energy transfer to the CT–π–π* and the π–π* states. The solid lines in the plots represent the results obtained from atomic transition densities (Eq. 6); the dotted lines are calculated using the point-dipole approximation (Eqs. 4,5). The inset shows the correction factor η.

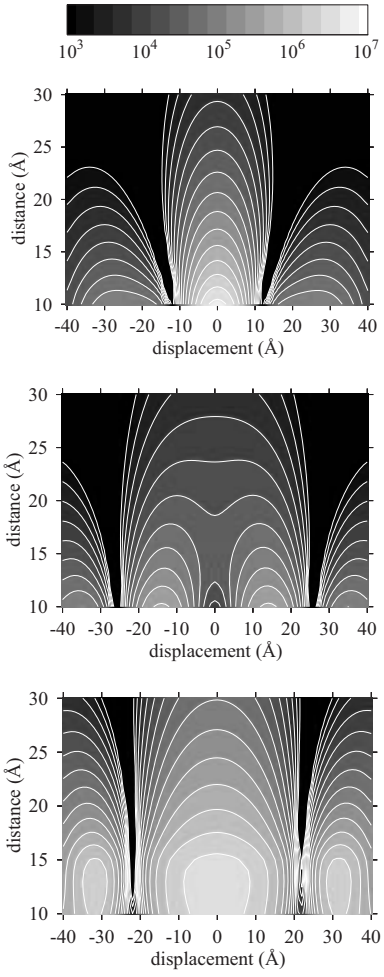

Figure 7. Dependence of the electronic coupling V^2 on molecular displacements in a cofacial configuration. The *x*-axis corresponds to lateral displacement of the oligomers along the long molecular axis, while the *y*-axis corresponds to increasing distances between the planes of the oligomers. The studied system for the upper and middle plots consists of a 4-ring LOPP donor and a 14-ring LOPPK acceptor. The upper plot corresponds to energy transfer to the localized CT–π–π* state and the middle plot to transfer to the delocalized π–π* state. The bottom plot describes energy transfer to a pristine 14-ring LOPP. The V^2 values are plotted on a logarithmic scale starting from 10^3 cm^{-2} (black region) up to values of 10^7 cm^{-2} (white region).

results suggest that the success of the point-dipole approximation, as implemented in the original Förster theory, to describe the excitation dynamics in disordered conjugated polymer films might simply arise from a cancellation of errors.

Finally, we discuss another case that nicely underlines the impact of the actual shape of the involved transition densities. Figure 7 collects the V^2 values obtained when varying the relative positions of the donor and acceptor oligomers in the cofacial configuration. The calculations are performed for the 4-ring LOPP donor and a 14-ring LOPPK acceptor. The horizontal axis corresponds to a longitudinal displacement of the centers of the coplanar oligomers, while the vertical axis refers to the inter-molecular distance. The top graph corresponds to energy transfer to the CT–π–π* state. It does not only quantitatively but also qualitatively differ from the central graph, which corresponds to energy transfer to the delocalized π–π* state. Most notably, for the case of transfer to the delocalized π–π* state, there exists an additional minimum for close separations between donor and acceptor when the oligomer centers are on top of each other (zero lateral displacement). This minimum is actually related to the very small transition densities for the π–π* state in the center of the ketone-containing chains (see lower part of Fig. 2). This is confirmed by the fact that when the results for energy transfer to ketone-containing chains are compared to those for transfer to a pristine (i.e., ketone-free) 14-ring LOPP (bottom part of Fig. 7), we find that in the latter case the minimum in the coupling is absent.

4. Conclusion

In conclusion, our results provide a clear illustration that the Förster model, which relies on a point-dipole approximation, can substantially fail in describing energy-transfer processes in conjugated polymers. We note that the failure of the model might sometimes be obscured by a cancellation of errors due to overestimated transfer rates for cofacial configurations and underestimated values for head-to-head configurations.

The key role played by the shape of the transition densities in the calculation of energy transfer rates has been described for several examples. Due to the significantly different electronic nature of the low-lying excited states in bridged poly(*para*-phenylenes) containing ketonic defects, it has been shown that the inadequacy of the Förster model is usually larger when studying energy transfer to (and from) delocalized excited states than when localized states are involved. In our studies we also find that applying the point dipole approximation results in a strong overestimation of the transfer rates for a cofacial conformation, while it results in an underestimation of the rates for a head-to-head configuration. The typical value for the correction factor of the Förster radius η in a head-to-head configuration is in the range between 1.1 and 1.6; for a cofacial configuration, η is in the range of 0.2 to 0.8.

5. Computational Details

The ground-state geometries of the donor and acceptor chromophores were computed at the Austin Model 1 (AM1) [24] level. To describe the relaxed geometry of the donor excited states, the AM1 Hamiltonian was coupled to a configuration interaction scheme (AM1-CI) [25]. The active space was chosen to contain the two highest occupied and two lowest unoccupied orbitals.

The electronic excitation energies, transition dipoles, and transition densities are calculated using the intermediate neglect of differential overlap Hamiltonian (INDO) [26] coupled to a single configuration interaction (CI) approach to include correlation effects. The size of the active CI space is scaled with the size of the molecule and consists of the 6*n* highest occupied and 6*n* lowest unoccupied orbitals (where *n* is the number of benzene rings).

To estimate the reliability of the distributed monopole method which uses the ZDO approximation, we also carried out calculations with the transition density cube method (Ref. [8]), which involves the full three-dimensional (3D) structure of the transition densities. The results were in very good agreement and no significant deviations from the distributed monopole method were observed.

In our calculations, we described the Coulomb interaction between the molecules by a $1/r$ potential (Eq. 6); using screened Coulomb potentials like Mataga-Nishimoto (MN) [27] would yield slightly different values but similar trends. We note that the MN potential is applied for instance, when deriving transfer rates from the half-splitting energies between the two lowest excites states in dimer configurations [11].

Received: March 16, 2004
Final version: June 23, 2004
Published online: December 20, 2004

[1] L. A. Staehelin, in *Photosynthesis III, Photosynthetic Membranes and Light Harvesting Systems* (Eds: L. A. Staehelin, C. J. Arntzen), Springer, Berlin, Germany **1986**, p. 1.

[2] G. D. Scholes, X. J. Jordanides, G. R. Fleming, *J. Phys. Chem. B* **2001**, *105*, 1640.

[3] a) C. W. Tang, D. J. Williams, J. C. Chang, *US Patent 5 294 870*, **1994**. b) S. Tasch, E. J. W. List, O. Ekström, W. Graupner, G. Leising, P. Schlichting, U. Rohr, Y. Geerts, U. Scherf, K. Müllen, *Appl. Phys. Lett.* **1997**, *71*, 2883.

[4] T. Virgili, D. G. Lidzey, D. D. C. Bradley, *Adv. Mater.* **2000**, *12*, 58.

[5] P. A. Lane, L. C. Palilis, D. F. O'Brien, C. Giebeler, A. J. Cadby, D. G. Lidzey, A. J. Campbell, W. Blau, D. D. C. Bradley, *Phys. Rev. B* **2001**, *63*, 235 206.

[6] A. Pogantsch, G. Trattnig, G. Langer, W. Kern, U. Scherf, H. Tillmann, H. H. Hörhold, E. Zojer, *Adv. Mater.* **2002**, *14*, 1722.

[7] E. J. W. List, R. Guentner, P. Scanducci de Freitas, U. Scherf, *Adv. Mater.* **2002**, *14*, 374.

[8] B. P. Krueger, G. D. Scholes, G. R. Fleming, *J. Phys. Chem. B* **1998**, *102*, 5378.

[9] a) J. N. Murell, J. Tanaka, *J. Mol. Phys.* **1964**, *7*, 634. b) M. Pope, C. E. Swenberg, *Electronic Processes in Organic Crystals and Polymers (Monographs on the Physics and Chemistry of Materials)*, Oxford University Press, Oxford, UK **1999**.

[10] D. Beljonne, J. Cornil, R. Silbey, P. Millié, J. L. Brédas, *J. Chem. Phys.* **2000**, *112*, 4749.

[11] W. Beenken, T. Pullerits, *J. Chem. Phys.* **2004**, *120*, 2490.

[12] D. Beljonne, G. Pourtois, C. Silva, E. Hennebicq, L. M. Herz, R. H. Friend, G. D. Scholes, S. Setayesh, K. Müllen, J. L. Brédas, *Proc. Natl. Acad. Sci. USA* **2002**, *99*, 10 982.

[13] G. D. Scholes, *Annu. Rev. Phys. Chem.* **2003**, *54*, 57.

[14] a) C. Ecoffet, D. Markovitsi, P. Millié, J. P. Lemaistre, *Chem. Phys.* **1993**, *177*, 629. b) S. Marquet, D. Markovitsi, P. Millié, H. Sigal, S. Kumar, *J. Phys. Chem. B* **1998**, *102*, 4697.

[15] B. P. Krueger, G. D. Scholes, G. R. Fleming, *J. Phys. Chem. B* **1998**, *102*, 5378.

[16] E. Zojer, A. Pogantsch, E. Hennebicq, D. Beljonne, J. L. Brédas, P. Scanducci de Freitas, U. Scherf, E. J. W. List, *J. Chem. Phys.* **2002**, *117*, 6794.

[17] L. Romaner, A. Pogantsch, P. Scandiucci de Freitas, U. Scherf, M. Gaal, E. Zojer, E. J. W. List, *Adv. Funct. Mater.* **2003**, *13*, 597.

[18] J. M. Lupton, M. R. Craig, E. W. Meijer, *Appl. Phys. Lett.* **2002**, *80*, 4489.

[19] X. H. Yang, D. Neher, C. Spitz, E. Zojer, J. L. Bredas, R. Güntner, U. Scherf, *J. Chem. Phys.* **2003**, *119*, 6832.

[20] J. M. Lupton, *Chem. Phys. Lett.* **2002**, *365*, 366.

[21] I. Franco, S. Tretiak, *Chem. Phys. Lett.* **2003**, *372*, 403.

[22] M. J. Mcintire, E. S. Manas, F. C. Spano, *J. Chem. Phys.* **1997**, *107*, 8152.

[23] For a head to head configuration between the two chromophores, η is equal to 1.38 (the distance between the centers is equal to the length of a single molecule); for a cofacial configuration one obtains $\eta = 0.53$ (the separation between the centers is chosen to be half of the length of one molecule).

[24] M. J. S. Dewar, E. G. Zoebisch, E. F. Healy, J. J. P. Stewart, *J. Am. Chem. Soc.* **1985**, *107*, 3902.

[25] *Ampac 5.0 User's Manual*, copyright 1994 Semichem, 7128 Summit, Shwanee, KS 66 216.

[26] M. C. Zerner, G. H. Loew, R. F. Kichner, U. T. Mueller-Westerhoff, *J. Am. Chem. Soc.* **1980**, *102*, 589.

[27] N. Mataga, K. Nishimoto, *Z. Phys. Chem. (Muenchen Ger.)* **1957**, *13*, 140.

